

Molecular Docking and 3D-QSAR Based Design of Novel Imidazopyridinone Derivatives as *Pseudomonas Aeruginosa* Thymidylate Kinase Inhibitors

S. VIKRAM KUMAR GOUD, P. SAI KIRAN REDDY,
S. SREE KANTH and M. VIJJULATHA*

Molecular Modeling and Medicinal Chemistry Group, Department of Chemistry,
Nizam College, Osmania University, Basheerbagh, Hyderabad-500 001, India
vijjulathamanga@gmail.com

Received 22 August 2013 / Accepted 4 October 2013

Abstract: Thymidylate kinase (TMK) is a potential chemotherapeutic target since it is directly involved in the synthesis of deoxythymidine 5'-triphosphate an essential component in DNA replication. Inhibiting the function of TMK blocks DNA synthesis in replicating organisms. We report 3D-QSAR analysis on a series of thymidine mimetics exhibiting potent inhibitory activity against TMK. Molecular docking, Comparative molecular field analysis (CoMFA) and comparative similarity indices analysis (CoMSIA) were carried out to determine the requisite 3D structural features required for potent thymidylate kinase inhibitory activity. The molecules were divided into training set and test set, a PLS analysis was performed and QSAR models were generated. The model showed good statistical reliability which is evident from the q^2_{loo} , r^2_{ncv} and r^2_{pred} . The models were graphically interpreted using CoMFA and CoMSIA contour maps. The results obtained from this study were used for rational design of potent inhibitors against thymidylate kinase.

Keywords: Thymidylate kinase, Thymidine triphosphate, Thymidine mimetics, Molecular docking, Comparative molecular field analysis, Comparative similarity indices analysis

Introduction

New antibacterial therapeutics that utilizes novel mechanism of action is urgently needed to combat growing resistance to existing antibacterial agents for both gram-positive and gram-negative infections. Although the discovery of new antibacterial classes is extraordinarily difficult¹, need is especially high for gram negative organisms prevalent, in hospitals and in particular for infections caused by *Pseudomonas aeruginosa*.

Pseudomonas aeruginosa is a gram negative bacterium and an opportunistic human pathogen. It mainly targets the immuno-compromised patients and typically infects the pulmonary tract, urinary tract and even causes blood infections. *P. aeruginosa* is highly

resistant to a wide range of antibiotics and disinfectants². This pathogen has been reported to have poorer outer membrane permeability to small molecules³, for which treatment options are often limited⁴⁻⁶.

Thymidylate kinase (TMK) has emerged as an attractive therapeutic target because inhibiting TMK functions blocks DNA synthesis in replicating organisms⁷. Thymidylate kinase (TMK, EC:2.7.4.9, ATP: phosphotransferase) belongs to the nucleoside monophosphate kinase (NMPK) family and catalyzes the reversible phosphorylation of dTMP to deoxythymidine 5'-diphosphate (dTDP) in the presence of ATP as its preferred phosphoryl donor⁸, situated at the junction of the de novo and salvage pathways for synthesis of deoxythymidine 5'-triphosphate (dTTP). TMK is the last specific enzyme in these pathways, therefore being essential for DNA replication & cell growth.

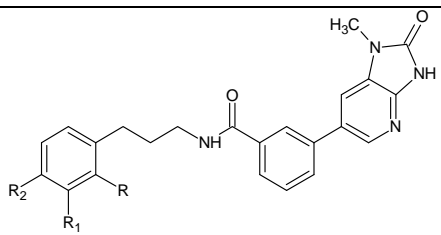
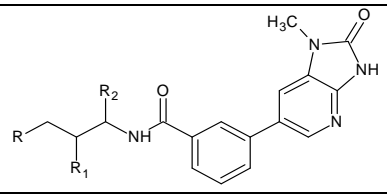
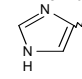
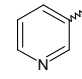
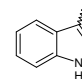
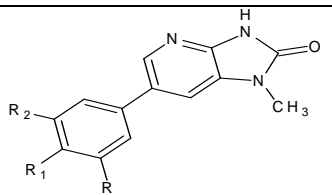
Biochemical and structural characterization of PaTMK has revealed subtle differences compared to the corresponding human isozyme (21% of sequence identity)⁹, it represents an attractive target for selectively inhibiting *Pseudomonas aeruginosa* DNA synthesis. Necessity for development of more potent and specific PaTMK inhibitors is an important task due to development of resistance by the organism against existing inhibitors. Recently Jun yong choi *et al.*¹⁰, reported imidazopyridinones as inhibitors of *Pseudomonas aeruginosa* targeting PaTMK, the inhibitors showed good hydrogen bond interactions with Thr101, Tyr104, Gln105 and Arg74. In an effort to design novel inhibitors of PaTMK several computational approaches are employed in development & optimization of inhibitors. In present article we report receptor based 3D-QSAR studies using CoMFA^{11,12} and CoMSIA¹³ methodologies on imidazopyridinones derivatives. PLS¹⁴ based statistical analysis was carried out on 40 molecules to identify the correlation. The contour maps generated enabled us to explain the observed variation in activity and guided us to design new molecules.

Methodology

A total of 40 molecules were available with reported IC₅₀ values for inhibition of paTMK¹⁰ and these values were converted to corresponding pIC₅₀ values (Table 1). The data set was divided into training and test set of 30 and 10 molecules respectively. All molecular modeling calculations were performed on a linux operating system. The crystal structure of PaTMK bound with 1-methyl-6-benzamido-imidazopyridinone inhibitor (PDB Id: 3UWO)¹⁰ was downloaded from protein data bank. GLIDE 5.6¹⁵ was used for molecular docking, protein was prepared using protein preparation module applying the default parameters and a receptor grid was generated around active site of PaTMK by selecting the cocrystallized ligand with receptor van der Waals¹⁶ scaling for non-polar atoms as 0.9. Molecules were built using maestro build panel and prepared by LigPrep application. Structures of molecules and their IC₅₀ and pIC₅₀ are given in Table 1. LigPrep produces low energy conformer of the ligand using the MMFF94s force field. These molecules were docked into the grid generated from TMK protein structures using standard precision docking mode¹⁶. Cocrystallised ligand was also docked and its root mean square deviation (RMSD) was calculated to validate the docking process. Dock pose of each ligand docked into the protein was analyzed for their hydrogen bond interactions with the receptor. Analysis of dock poses of all molecules showed similar hydrogen bond interactions with Arg74, Thr101, Tyr104 and Gln105 of active site residues.

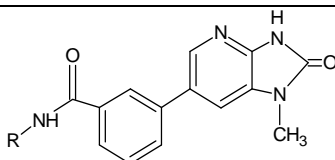
Overlay of the most promising poses (best glide score along with most physiologically similar positions) has been taken directly into 3D-QSAR analysis in this way QSAR is taken a step beyond what is usually done in such analysis. Overlay of dock pose of each ligand is shown in Figure 1.

Table 1. Structure of PaTMK inhibitors along with IC₅₀, pIC₅₀, predicted pIC₅₀ and Dock Score

Molecule	R	R ₁	R ₂	IC ₅₀ μM	pIC ₅₀	Predicted pIC ₅₀		Dock Score kcal/mol
						CoMFA	CoMSIA	
								
1	H	H	H	0.12	6.920	6.703	6.623	-10.651
2*	H	H	F	0.12	6.920	6.551	6.577	-10.890
3*	H	H	CF ₃	0.16	6.795	5.451	5.938	-10.979
4	-CO ₂ CH ₃	H	H	0.37	6.431	6.494	6.496	-10.902
5*	H	H	-CH ₂ NH ₂	3.2	5.498	6.093	6.228	-10.684
6	H	-CH ₂ NH ₂	H	2.2	5.657	5.669	5.618	-10.772
7*	H	COOH	H	2.4	5.619	5.710	5.687	-10.537
8	H	H	COOH	2.7	5.568	5.738	5.617	-10.691
9	COOH	H	H	2.0	5.698	5.871	5.739	-11.177
								
10*	Ph	COOH	H	0.25	6.602	5.783	5.582	-9.612
11	-C ₅ H ₉	H	H	0.81	6.091	6.112	6.583	-10.194
12		H	H	0.99	6.004	6.054	5.926	-10.366
13		H	H	0.51	6.294	6.204	6.171	-10.398
14		H	H	0.20	6.698	6.564	6.718	-11.388
								
15	H	H	H	58	4.236	4.429	4.322	-9.089
16	OH	H	H	11	4.958	4.790	4.877	-9.358
17	NH ₂	H	H	63	4.200	4.278	4.326	-9.533

Contd...

18	CH ₂ OH	H	H	37	4.431	4.231	4.336	-9.652
19	H	H	C(O)N(CH ₃) ₂	104	3.982	4.101	4.142	-9.913
20	H	H	-NHC(O)CH ₃	3.4	5.468	5.631	5.563	-10.148
21	H	H	-C(O)CH ₃	13	4.886	4.970	4.496	-10.037
22	H	OH	H	21	4.677	4.754	4.734	-10.278
23	H	-CH ₂ NH ₂	H	4.9	5.309	4.806	5.296	-9.642



24*	-CH ₃	2.2	5.657	5.027	5.488	-10.238
25	-CH ₂ C(O)NH ₂	0.88	6.055	6.119	5.879	-10.463
26*	-CH ₂ C(O)OH	0.88	6.055	5.579	5.698	-10.510
27	-CH ₂ CH ₂ S(O) ₂ OH	1.3	5.886	5.936	5.873	-10.125
28	-CH ₂ CN	2.1	5.677	5.552	5.605	-10.322
29		2.3	5.638	5.578	5.498	-9.918
30	-CH ₂ CH ₂ C(O) OH	2.6	5.585	5.770	5.634	-10.865
31	-CH ₂ CH ₂ OH	2.6	5.494	5.656	5.444	-10.436
32	-CH ₂ CH ₂ N ⁺ H ₃	3.2	5.850	5.671	5.818	-9.670
33	-(CH ₃)CHCOOH	5.0	5.301	5.176	5.360	-10.168
34		2.0	5.698	5.838	5.795	-10.105
35*	-CH ₂ CH ₂ Ph	2.9	5.537	5.389	4.968	-9.843
36*		3.0	5.522	5.686	5.980	-11.023
37		6.2	5.207	5.142	5.327	-10.127
38		68	4.167	4.088	4.103	-9.282
39*		66	4.180	4.535	4.210	-9.690
40		152	3.818	3.972	3.981	-9.155

*represent test set of molecules

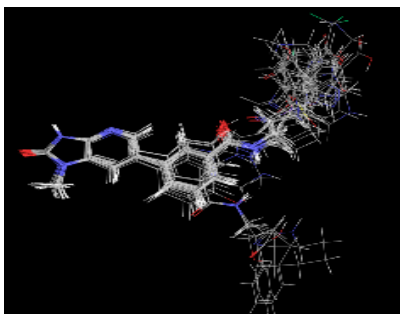


Figure 1. Dockpose alignment of TMK inhibitors

Molecules were imported into SYBYLX-1.2 molecular modeling program package¹⁷, Gasteiger-Huckel¹⁸ charges were assigned. Standard Tripos force fields were employed for CoMFA and CoMSIA analysis. A 3D cubic lattice of dimension 4 Å in each direction with each lattice intersection of regularly spaced grid of 2.0 Å was created. Steric and electrostatic parameters were calculated in CoMFA fields while hydrophobic, acceptor and donor parameters in addition to steric and electrostatic were calculated in CoMSIA fields at each lattice intersection of regularly spaced grid of 2.0 Å was created. The sp³ carbon atom was used as a probe atom to generate steric (Lennard-jones potential) field energies and a charge of +1 to generate electrostatic (columbic potential) field energies. A distance dependent dielectric constant of 1.00 was used. Steric and electrostatic fields were truncated at +30.00 kcal/mol. The similarity indices descriptors were calculated using the same lattice box employed for CoMFA calculations using sp³ carbon as a probe atom with a +1 charge, +1 hydrophobicity & +1 hydrogen bond donor and +1 hydrogen bond acceptor properties.

A PLS regression was used to generate a linear relationship that correlates changes in the computed fields with changes in corresponding experimental values of biological activity (pIC₅₀) for the data set of ligands. Forty molecules were divided into training and test set. Biological activity values of ligands were used as dependent variables in PLS statistical analysis. Column filtering value(s) was set to 2.0 kcal/mol to improve the signal-to-noise ratio by omitting those lattice points whose energy variations were below the threshold. Cross-validations were performed by leave -one -out [LOO] procedure to determine the optimal number of components (ONC) and coefficient q²_{loo}. ONC obtained are then used to derive the final QSAR model using all the training set compounds with non-cross validation and to obtain conventional correlation coefficient (r²_{ncv}). To validate CoMFA and CoMSIA derived models, the predictive ability for the test set of compounds (expressed as r²_{pred}) was determined by using the following equation.

$$r^2_{\text{pred}} = (\text{SD-PRESS})/\text{SD}$$

SD is the sum of squared deviations between biological activities of test set molecules and mean activity of the training set. PRESS is sum of squared deviation between observed & predictive activities of the test set molecules. Since the statistical parameters were found to be the best for further predictions of the designed molecules. The designed molecules were also constructed, minimized and docked into the protein active site, as mentioned above.

Results and Discussion

TMK inhibitors, shown in Table 1 along with IC₅₀ and pIC₅₀ values, were docked into the active site; they showed five hydrogen bond interactions with the active site residues. Accuracy of docking protocol was evaluated by redocking the crystal structure ligand and its

RMSD from the experimental binding mode determined by x-ray crystallography was calculated, and it gave a value of 0.4803 Å (Figure 2). The correlation between dock score (glide score) and pIC_{50} gave a correlation coefficient value (r) of 0.693, which shows appreciable relation between biological activity and docking, scatter plot of pIC_{50} and glide score is shown in Figure 3.

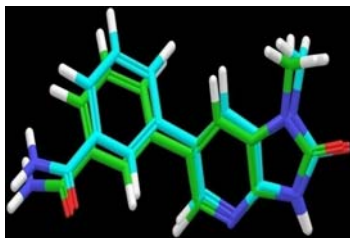


Figure 2. Superimposition of crystal structure pose (cyan) on docked pose (green) of co-crystallized ligand

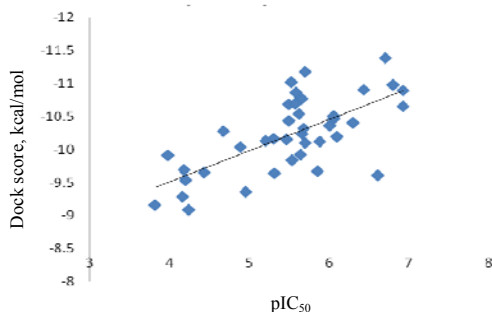


Figure 3. Scatter Plot of pIC_{50} vs. Dock Score

Molecules having specific hydrogen bond interactions with active site of the receptor, where imidazopyridinone C=O act as hydrogen bond acceptor to Arg74, Thr101, while both –NH of cyclic imidazopyridinone ring act as donor and acceptor to C=O group of Gln105 and benzamido C=O act as hydrogen bond acceptor to –OH of Tyr104 in TMK, were considered. The 3D-QSAR, CoMFA and CoMSIA analysis were carried out in the reported inhibitors (Table 1). Molecules having precise IC_{50} values were selected and those that did not show interactions with the protein active site (via docking) were removed from the data set.

A set of 40 molecules were used for derivation of model, these were divided into a training set of 30 molecules & test set of 10, keeping in view that the activity range is with a minimum of 3 log units differences in both the sets. CoMFA & CoMSIA statistical analysis is summarized in Table 2. Statistical data shows q^2_{loo} 0.577 for CoMFA 0.670 for CoMSIA models, r^2_{ncv} of 0.961 and 0.962 for CoMFA & CoMSIA, respectively, which indicates a good internal predictive ability of models. To test the predictive ability of models, a test set of 10 molecules exchanged from the model derivation was used. The predictive correlation coefficient r^2_{pred} of 0.521 for CoMFA and 0.603 for the CoMSIA models indicate good external predictive ability for the models. Scatter plot for actual and predicted pIC_{50} values for CoMFA and CoMSIA studies shown in Figure 4. The CoMSIA model showed better results than CoMFA model, this shows that the hydrophilic and hydrophobic fields which were not included in the CoMFA model are important for explaining the potency of the molecules. This is also evident from the docking results. The predicted activity and glide scores of the molecules are provided in Table 1.

Table 2. Summary of PLS results

Statistical parameters	CoMFA	CoMSIA
q^2_{loo}	0.577	0.670
No. of molecules in training set	30	30
No. of molecules in test set	10	10
ONC	5	4
SEE	0.176	0.168
r^2_{ncv}	0.961	0.962
F_{ratio}	116.750	159.649
r^2_{pred}	0.521	0.603
Fraction of field contributions		
Steric	72.8	20.1
Electrostatic	27.2	7.8
Hydrophobic	--	18.9
Donor	--	33.3
Acceptor	--	19.9

q^2_{loo} : Cross-validated correlation coefficient by leave one out method; r^2_{ncv} : non-cross-validated correlation coefficient; r^2_{pred} : predictive correlation coefficient on test set; SEE: standard error of estimate; F_{ratio} : Fischer test value; ONC: optimal Number of principal components

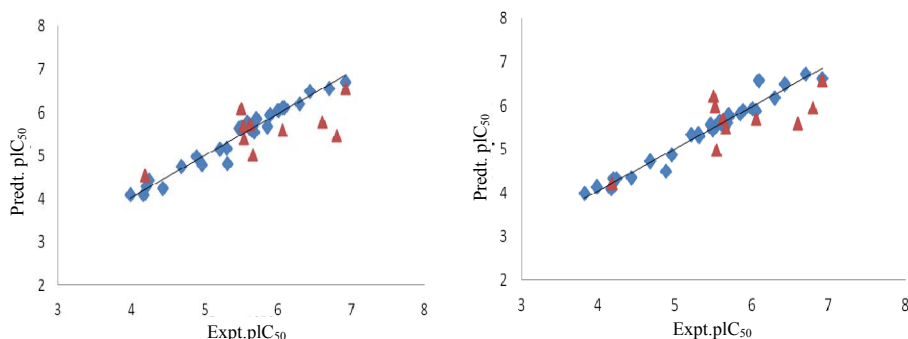


Figure 4. Graphs of the experimental *versus* predicted pIC_{50} values of the training (♦) and test (▲) compounds from the CoMFA and CoMSIA models

CoMFA and CoMSIA contour maps

To visualize the information content of the derived 3D-QSAR models, CoMFA and CoMSIA contour maps were generated. The Contour plots are representation of the lattice points & the difference in the molecular field values, at lattice points, strongly connected with difference in the receptor binding affinity. Molecular fields define favorable or unfavourable interaction energies of aligned molecules with a probe atom traversing across lattice points suggests modification required to design new molecules. Contour maps of CoMFA denote region in the space where molecules would favourably or unfavourably interact with the receptor while CoMSIA contour maps denote those areas within the specified region where presence of a group with a particular physicochemical activity binds to the receptor. CoMFA and CoMSIA results were graphically interpreted by field contribution maps using “STDEV*COEFF” field type. All contours represented default 80 and 20% level contribution for favoured and disfavoured regions.

The most potent analogue, molecule 1 was embedded in the map Figure 5(a, b), to demonstrate its affinity for steric and electrostatic regions of inhibitors. The areas of yellow indicate regions of steric hindrance to activity, while green areas indicate a steric contribution to potency. The blue regions indicate a positive electrostatic charge potential associated with increased activity, while red region show negative charge potential. The steric contour maps of CoMFA show, the green regions surrounding alkyl linker attached to benzene ring for substitution of sterically bulky favoured groups. The yellow contour over the benzamide ring suggests steric bulk disfavoured region in molecule 1. Electrostatic contour maps shows two regions of blue contours above amide group and at *para* position of benzene ring attached to the alkyl chain for positive electrostatic potentials, a red contour is seen near the meta position of both the phenyl rings in molecule 1 suggesting substitution of more negatively charged substituents at this position will significantly improve biological activity.

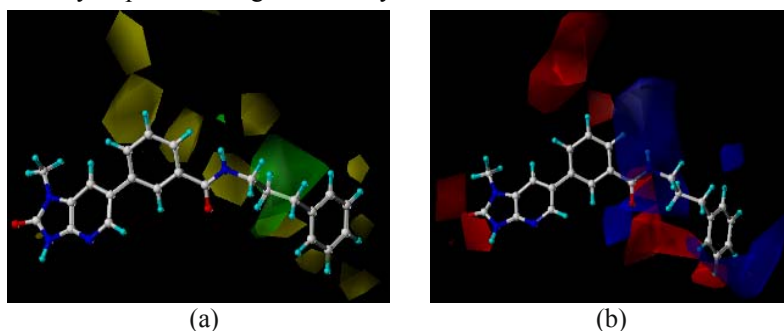


Figure 5. CoMFA steric standard deviation (S.D.* coefficient) contour maps illustrating steric (a) and electrostatic (b) features in combination with molecule 1. Green contours show favourable bulky group substitution at that point while yellow regions show disfavourable bulky group substitution for activity. Red contours indicate negative charge favouring activity, whereas blue contours indicate positive charge favouring activity

Figure 6(a-e) shows the contour maps derived from the CoMSIA PLS model. The most potent analogue, molecule 1, was embedded in the maps to demonstrate its affinity for the steric, electrostatic, hydrophobic, hydrogen bond donor and acceptor regions of inhibitors. The steric map is similar to the CoMFA steric map showing favoured and disfavourable regions. In steric contour embedded by molecule 1 the benzyl group is penetrating into the green region for bulky favoured substitution and the entire molecule is away from the disfavourable yellow region. The electrostatic contour map shows a red contour over the carbonyl of benzamide ring in molecule 1 indicating a negative electrostatic potential. The blue regions over the $-NH$ of amide, CH_2 attached to benzene ring indicates regions with positive electrostatic potentials in molecule 1. The hydrophobic contours shows, meta and para positions of benzene ring incorporated into the favoured yellow region suggests substituting sterically bulky, hydrophobic groups further increases biological activity. A white contour is observed around the alkyl linker region suggesting hydrophilic substitution on the linker region will increase activity. The donor contour map show benzamide group incorporated into disfavourable purple regions in molecule 1. The acceptor contour maps shows favoured magenta region near to the carbonyl group, disfavourable red region is observed on to the nitrogen of amide and *para* position of benzene ring suggesting substitution with acceptor groups will increase the potency.

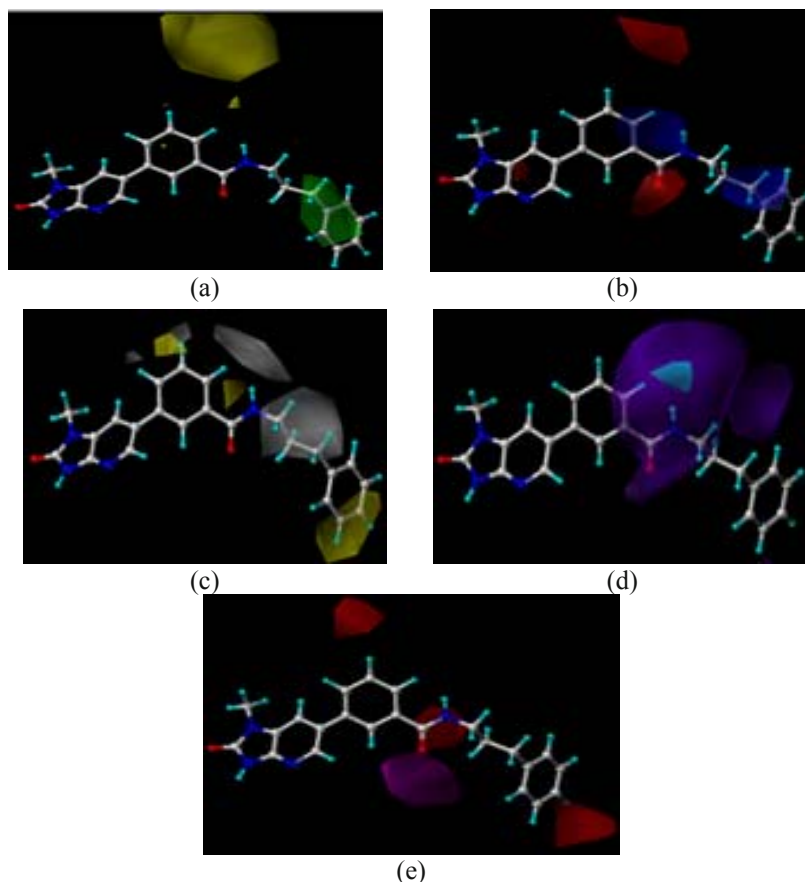


Figure 6. CoMSIA SD* coefficient contour maps in combination with molecule 1 illustrating features (a) Steric: Green contours represent favourable bulky group substitution at that point while yellow regions are disfavorable for activity; (b) Electrostatic: Red contours indicate negative charge favouring activity, whereas blue contours indicate positive charge favouring activity; (c) Hydrophobic: Yellow contour represent hydrophobic favoured region, white indicates the hydrophilic favoured regions; (d) Donor: The purple contour represents *H*-bond donor disfavoured regions while cyan indicates *H*-bond donor favoured and (e) Acceptor: Magenta and red contour represent *H*-bond acceptor disfavoured and favoured regions.

Detailed contour map analysis of both CoMFA and CoMSIA models empowered us to identify structural requirements for observed inhibitory activity (Figure 8). The molecules were modified to further improve the inhibition activity towards PaTMK. Molecule 1 was chosen as a reference structure to design molecules (Table 3) with increased potency. New molecules designed were docked into the protein active site and they showed similar interactions with comparable dock scores and dock poses were used to predict the activity by applying the 3D-QSAR model. The new molecules showed better predicted activity with respect to the most active molecule. Sterically bulky & hydrophobic groups (ethyl, *t*-butyl, *n*-butyl, benzyl) substituted on CH₂ of alkyl linker region attached to benzene ring and also hydrophilic groups (OH, COOH, SCH₃) substituted on meta position of benzene ring attached to the amide group increased the activity.

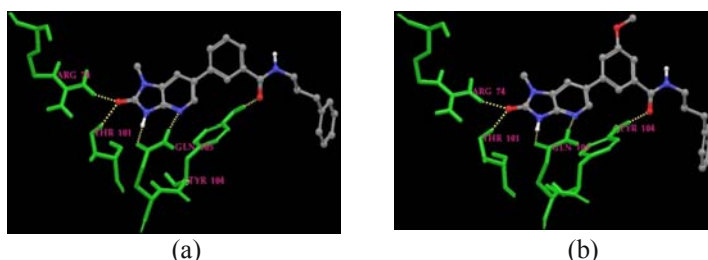


Figure 7. Docked pose of (a) molecule 1 and (b) molecule N5 in the protein active site showing similar hydrogen bond interactions with Arg 74, Thr 101, Gln 105, and Thr 104

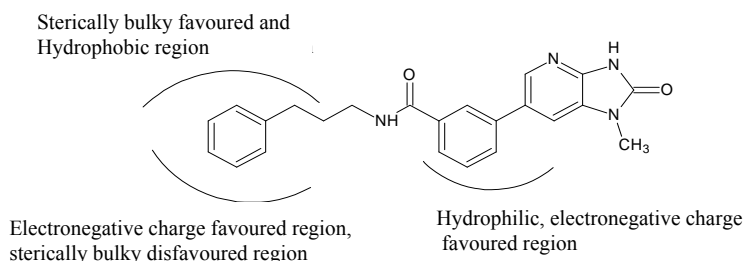


Figure 8. Structural requirements for PaTMK inhibitors obtained from CoMFA (CF) and CoMSIA (CMS) contour map analysis

Table 3. Structure, predicted pIC₅₀ and dock score of designed molecules

Molecule							Pred pIC ₅₀	Pred pIC ₅₀	DockScore kcal/mol
	R ₁	R ₂	R ₃	R ₄	R ₅	R ₆	CoMFA	CoMSIA	
N1	H	H	H	ethyl(R)	H	H	7.208	6.438	-10.546
N2	H	t-butyl	H	H	H	H	6.521	6.965	-10.576
N3	Cl	H	H	H	-S(CH ₃)	H	7.139	5.815	-10.825
N4	OH	H	H	H	-S(CH ₃)	H	7.377	5.951	-10.911
N5	H	H	H	H	H	OH	7.113	6.673	-10.989
N6	H	H	H	H	H	COOH	6.903	7.090	-10.645
N7	H	H	-CH ₂ Ph	-CH ₂ Ph	H	H	6.736	7.119	-11.476
N8	H	H	H	H	H	-O(pr)	7.567	6.645	-10.455
N9	n-butyl	H	H	ethyl(R)	H	-S(CH ₃)	6.967	6.535	-9.365
N10	-CHCl ₂	H	H	H	-S(CH ₃)	H	7.102	5.629	-10.851
N11	H	H	H	H	-S(CH ₃)	H	7.311	5.783	-10.695
N12	F	H	H	H	-S(CH ₃)	H	7.275	5.795	-11.183
N13	H	H	H	n-butyl(R)	H	OH	7.452	6.799	-10.851
N14	ethyl	H	H	Ethyl(R)	H	OH	7.062	6.727	-10.395

Conclusion

Molecular docking based 3D-QSAR studies are widely used tools for understanding binding modes of the molecule to the protein receptors and rationalize structural requirements for the inhibitory activity of the molecules. CoMFA & CoMSIA methodologies were used to build models for PaTMK inhibitory activity of imidazopyridinone derivatives. The generated models have statistical reliability that is evident from high r^2 and q^2 values for all the models. Based on detailed contour map analysis improvement in PaTMK binding affinity can be achieved through conformationally restricted substitution on CH_2 of alkyl linker region attached to benzene ring and *meta* position of benzene ring attached to the amide group. The designed molecules based on these parameters showed better predictive activity than reference molecule, this indicates QSAR models generated have good predictive ability to design potent inhibitors. These molecules can be synthesized to generate a greater number of molecules with required pharmacokinetics for further clinical studies.

Acknowledgement

We gratefully acknowledge support for this research from Department of Science and Technology, New Delhi, India, University Grants Commission, New Delhi, India and Department of chemistry, Nizam College, Hyderabad, India. We also acknowledge Schrödinger Inc. for GLIDE software, Tripos Inc. for SYBYLX-1.2.

References

1. Payne D J, Gwynn M N, Holmes D J and Pompliano D L, *Nat Rev Drug Dis.*, 2007, **6**(1), 29; DOI:10.1038/nrd2201
2. Stover C K, Pham X Q, Erwin A L, Mizoguchi S D, Warren P, Hickey M J, Brinkman F S, Hufnagle W O, Kowalik D J, Lagrou M, Garber R L, Goltry L, Tolentino E, Westbrook W S, Yuan Y, Brody L L, Coulter S N, Folger K R, Kas A, Larbig K, Lim R, Smith K, Spencer D, Wong G K, Wu Z, Paulsen I T, Reizer J, Saier M H, Hancock R E, Lory S and Olson M V, *Nature*, 2000, **406**, 959.
3. Mdululi K E, Witte P R, Kline T, Barb A W, Erwin A L, Mansfield B E, McClerren A L, Pirrung M C, Tumey L N, Warren P, Raetz C R H and Stover C K, *Antimicrob Agents Chemother.*, 2006, **50**(6), 2178-2184; DOI:10.1128/AAC.00140-06
4. Obritsch M D, Fish D N, MacLaren R and Jung R, *Pharmacotherapy*, 2005, **25**(10), 1353-1364.
5. Rice L B, *Curr Opin Microbiol.*, 2009, **12**(5), 476-461; <http://dx.doi.org/10.1016/j.mib.2009.08.001>
6. Rice L B, *Cleve Clin J Med.*, 2007, **74**(4), S12; DOI:10.3949/ccjm.74.Suppl_4.S12.
7. Kandeel M, Kato A, Kitamura Y and Kitade Y, *Nucleic Acids Symp Ser.*, 2009, **53**(1), 283-284; DOI:10.1093/nass/nrp142
8. Anderson E, Nucleoside and Nucleotide Kinases. In the Enzymes 3rd Ed., Academic Press: New York, 1973, 8, 49; ISBN-10: 0121227103
9. Munier-Lehmann H, Chafotte A, Pochet S and Labesse G, *Protein Sci.*, 2001, **10**(6), 1195-1205; DOI:10.1110/ps.45701
10. Choi J Y, Plummer M S, Starr J, Desbonnet C R, Soutter H, Chang J, Miller J R, Dillman K, Miller A A and Roush W R, *J Med Chem.*, 2012, **55**(2), 852-870; DOI:10.1021/jm201349f
11. Cramer R D, Patterson D E and Bunce J D, *J Am Chem Soc.*, 1988, **110**(18), 5959-5967; DOI:10.1021/ja00226a005.

12. Cramer III R D, Patterson D E, Ildiko E. Frank and Bunce J D, *Quant Struct Act Relat.*, 1988, **7(1)**, 18-25; DOI:10.1002/qsar.19880070105
13. Klebe G, Abraham U and Mietzner T, *J Med Chem.*, 1994, **37(24)**, 4130-4146; DOI:10.1021/jm00050a010
14. Wold S, Johansson A and Cochi M, PLS-Partial least squares projection to latent structures. Lieden: ESCOM, 1993, 523-550.
15. Schrödinger, LLC, New York: Glide Version 5.6, 2010
16. Friesner R A, Banks J L, Murphy R B, Halgren T A, Klicic J J, Mainz D T, Repasky M P, Knoll E H, Shelley M, Perry J K, Shaw D E, Francis P and Shenkin P S, *J Med Chem.*, 2004, **47(7)**, 1739-1749; DOI:10.1021/jm0306430
17. Sybyl-X1.2, Tripos Associates, St. Louis (MO), 2010.
18. Gasteiger J and Marsili M, *Tetrahedron*, 1980, **36(22)**, 3219-3228; [http://dx.doi.org/10.1016/0040-4020\(80\)80168-2](http://dx.doi.org/10.1016/0040-4020(80)80168-2)